ACS APPLIED MATERIALS & INTERFACES

Research Article

www.acsami.org

Electric Double Layer Formed by Polarized Ferroelectric Thin Films

Robert J Ferris,[‡] Shihong Lin,[†] Mathieu Therezien,[†] Benjamin B. Yellen,[‡,#] and Stefan Zauscher*[,‡]

[‡]Department of Mechanical Engineering and Material Science, Duke University, 144 Hudson Hall, Durham, North Carolina 27708, United States

[†]Department of Civil Engineering, Duke University, 121 Hudson Hall, Durham, North Carolina 27708, United States

[#]University of Michigan-Shanghai Jiao Tong University, Joint Institute, 800 Dong Chuan Road, Shanghai, People's Republic of China

Supporting Information

ABSTRACT: Ferroelectric surfaces can have very high surface charge densities that can be harnessed for manipulation of charged colloidal particles and soft matter in aqueous environments. Here, we report on the electrical double layer (EDL) formed by polarized ultrasmooth lead zirconium titanate (US-PZT) thin films in dilute electrolyte solutions. Using colloidal probe force microscopy (CPFM) measurements, we show that the ion distribution within the double layer can be changed by reversing the ferroelectric polarization state of US-PZT. The interaction force in dilute 1:1 electrolyte solution between the negatively charged probe and a positive surface charge (upward polarized) US-PZT thin film is attractive, while the interaction force is repulsive for a negative surface charge (downward polarized) film. We modeled these interactions with a constant-potential EDL model between dissimilar surfaces with the inclusion of a Stern layer. We report the surface potentials at the inner and outer-Helmholtz planes both for polarization states and for a range of ionic strength solutions. Effects of free-charge carriers, limitations of the analytical model, and effects of surface roughness are discussed.

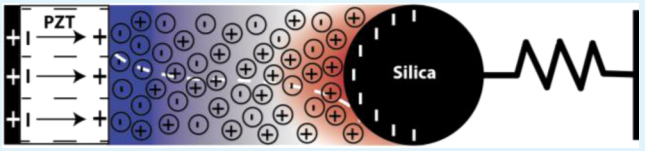

KEYWORDS: *interfacial forces, colloidal probe force microscopy, lead zirconium titante, PZT, electrolyte solution, surface charge*

INTRODUCTION

Ferroelectric thin films (FETFs) belong to a class of materials that can maintain an electric polarization state in the absence of an externally applied electric field.[1−3] The film's polarization state and the resulting surface charge density originate from a bistable, switchable dipole moment, maintained across the ferroelectric domains of the material.[2,4] The charge density on the exposed surface of a polarized FETFs is equal to the normal component of the remnant polarization vector ($\sigma_{FETF} = \vec{P} \cdot \hat{n}$). The net surface charge density can be induced to be either positive or negative depending on the direction of the applied polarizing electric field.[5−7]

The ability to control the remnant polarization state has led to the widespread use of ferroelectrics in a range of semiconductor-based devices.[3,8,9] Recently, new sensing applications for ferroelectrics have been proposed where the polarization state of the FETF can influence interfacial forces in liquid environments.[10] FETFs ability to control electrical double layer (EDL) formation has a wide range of potential applications, including, interfacial sensing,[11] microfabrication,[12] and micromixing.[13] Figure 1A is a schematic of the EDL structure between a native, nonpolarized FETF with a positive surface charge and a negatively charged colloidal probe in an aqueous environment. The interactions between the oppositely charged surfaces give rise to interfacial attraction. Figure 1B,C shows a polarized FETF expressing a net negative surface charge or net positive surface charge, respectively. Here, the uncompensated charge at the top surface of the FETF induces EDL formation. Because of the high ferroelectric surface charge densities, a Stern layer forms at the FETF−liquid interface. The outer-Helmholtz plane (OHP) is indicated by the dotted line. At the bottom surface, the polarization charge is compensated by free charges held in the bottom, metal electrode.

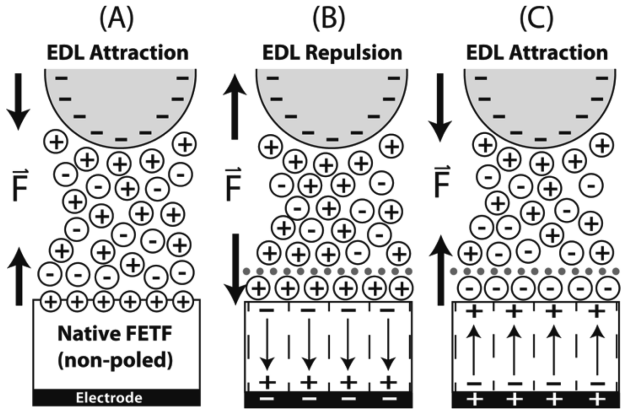

Figure 1. Schematic showing the electric double layer structure and interaction force between a negatively charged colloidal probe and (A) a native, nonpoled FETF with a positive native surface charge, (B) a polarized FETF with a negative surface charge, and (C) a polarized FETF with a positive surface charge.

Received: January 3, 2013
Accepted: March 13, 2013
Published: March 13, 2013

Although switching of the polarization direction induces a change in the EDL counterion distribution, there are still significant challenges for operating FETFs in aqueous environments. We found that careful selection of the substrate and the processing conditions during FETF fabrication can increase FETF stability in aqueous environments by reducing in-plane stress, surface roughness, and crack formation. Our results demonstrate how the FETF polarization state influences interfacial forces in aqueous environments and highlights the potential of FETFs to mediate surface forces.

Surface charges for common oxides typically arise from proton exchange or ion-complexation reactions between the ions in solution and surface sites.[14−16] For polarized, perovskite-based FETFs in aqueous environments, the effective surface charge density is due to the combination of the polarization induced surface charge (σ_F) and the surface charge density of the native oxide layer (σ_S) (eq 1)

$$\sigma_T = \sigma_F + \sigma_S \quad (1)$$

The relative magnitudes of these two surface charge contributions, however, can differ greatly. The surface charge density for a typical oxide surface is limited by the number of reactive surface site densities, which are typically on the order of 0.1 μC cm^{-2}.[8,17−19] Alternatively, FETFs such as lead zirconium titanate (PZT) can maintain surface charge densities that are several orders of magnitude higher (values can exceed 30 μC cm^{-2}),[8,17−19] which implies that the charge density of a polarized FETF film should dominate over the native surface charge density.

Our use of ultrasmooth, 52/48 lead zirconium titanate (US-PZT) thin films for control over electric double layer formation requires fabrication of FETFs that have nanometer scale mean surface roughness and high remnant polarization and are stable in aqueous environments. Figure 2A shows a typical hysteresis

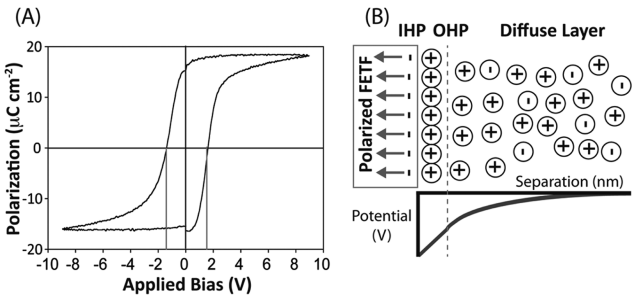

Figure 2. (A) Hysteresis loop of our 52/48 US-PZT thin film. Remnant polarization values are −16.3 and 15.3 μC cm^{-2}; the coercive field values are −146.5 and 155.2 kV/cm. (B) Schematic of the electric double layer structure above a polarized FETF with a negative surface charge in a dilute electrolyte solution and a corresponding sketch of the potential profile.

curve for our US-PZT thin films. Because the high surface charge of the polarized US-PZT thin films will result in high surface potentials, it is reasonable to assume that the EDL structure is partitioned into a Stern layer and a diffuse double layer of counterions. The inclusion of a Stern layer is consistent with EDL modeling of surfaces that have a high charge density in solution[20−22] and has been reported for polarized PZT surfaces in solution (Figure 2B).[23] Within the Stern layer, the condensed sheet of counterions is energetically trapped proximal to the solid−liquid interface, and the layer can be modeled as a parallel plate capacitor.[24] In the adjacent diffuse double layer, however, the ions are modeled as a distributed cloud where both the ion concentration and the electric potential decay exponentially with increasing distance away from the surface.[24] Since ferroelectric hysteresis properties can be accurately measured before the FETF is placed in solution, the effective surface charge density at the inner-Helmholtz plane (IHP of Figure 2B) of the Stern layer is known. The remaining surface charge (or potential), measured at the outer-Helmholtz plane of the Stern layer (OHP of Figure 2B), represents the boundary condition for the adjacent diffuse double layer region.

The study of electric double layer (EDL) formation has been driven by applications ranging from colloidal stability (e.g., aggregation[25] and filtration[26]) to interfacial sensing (e.g., biosensors[27] and lab-on-a-chip development[28]).[29] Although a deeper understanding of interfacial forces has led to improvements in interfacial engineering, it is still difficult to determine the effective charge density of a surface in solution because it usually depends on an equilibrium reaction between the surface sites and the surrounding environment, which in turn depend on solution conditions such as pH,[30−32] ionic strength,[21,33,34] or ion type.[20,35] Additionally, any attempt to change the surface charge density, through either functionalization or chemical treatment, invariably results in an unquantifiable change in the surface charge density at the inner Helmholtz plane (IHP). In contrast, ferroelectrics have the unique property of maintaining either a positive or negative surface charge density independent from the solution conditions or by chemical modification. Additionally, the surface charge density of a FETF can be experimentally determined prior to exposure, which allows for better estimation of the potential at the IHP. These advantages suggest that ferroelectric surfaces can significantly advance the study of EDLs.

We present, for the first time, the experimental measurement of an electric double layer induced by the remnant polarization state of a FETF in water. Using colloidal probe force microscopy (CPFM), we measured the EDL interaction force as a function of separation distance between a negatively charged colloidal probe (borosilicate sphere) and ultrasmooth PZT (US-PZT) surfaces over a range of ionic strengths. We demonstrate that the polarization state of the FETF dominates the net surface charge and thus the interaction force. Furthermore, the comparison of experimental and theoretical modeling of the EDL interactions reveals that the theoretically predicted IHP surface charge density matches the measured ferroelectric remnant polarization of the US-PZT film. Our observations motivate the continued development of FETF for interfacial-sensing applications.

MATERIALS AND METHODS

Substrate Preparation. Silicon wafers (⟨100⟩, Virginia Semiconductor) were first cleaned by sonication for 10 min in 0.5% sodium dodecyl sulfate (SDS) solution, followed by rinsing 10 times with Milli-Q grade water (18.2 MΩ·cm). The wafers were then immersed for 20 min in 3:1 H_2O_2/H_2SO_4 (Piranha solution), followed by being rinsed 10 times with Milli-Q grade water, and finally dried in a stream of N_2. (*CAUTION*: "Piranha" solution reacts violently with organic materials; it must be handled with extreme care.)Next, 200 nm of titanium and 100 nm of platinum were deposited onto the wafer surface using a Kurt Lesker PVD 75 e-beam source evaporator at ∼4 × 10^{-5} Torr.

Sol−Gel Synthesis. US-PZT thin-films with a Zr/Ti atomic ratio of 52/48 were fabricated from a sol−gel precursor (17 wt % Type E1 with relative atomic ratio: 125/52/48 Pb/Zr/Ti, Mitsubishi Materials

Corp). The excess lead was added to the sol−gel precursor to compensate for the loss of lead oxide during final film annealing.[36] The sol−gel solution was stored under dry conditions at 5 °C and protected from light. Prior to deposition, the sol−gel was warmed to room temperature and sonicated for 15 min. The precursor was passed through a 0.1 μm filter and deposited onto a platinum-coated silicon substrate, making sure to completely cover the substrate surface. The sol−gel precursor was then spin-coated using a two-stage ramp profile (5 s spin at 500 rpm followed by 40 s at 3000 rpm). Next, the solvent was evaporated on a hot plate of 90 °C for 120 s. The films were then pyrolized in a Thermolyne Benchtop annealing furnace at 450 °C for 35 min followed by cooling at a rate of 0.5 °C s^{-1}. Finally, the films were annealed using a rapid thermal annealer (Jipelec JetFirst 100) at 700 °C for 15 s. This fabrication process resulted in ultrasmooth PZT thin films with mean thickness of ∼116 nm and RMS roughness of ∼2.4 nm. All US-PZT samples were annealed immediately prior to measurement.

Ferroelectric Property Testing. The dielectric constant and remnant polarization of our US-PZT thin films were measured with a Radiant RT66b ferroelectric tester using circular platinum capacitors (50 μm diameter) evaporated onto the US-PZT surface. The platinum capacitors were annealed at 350 °C for 15 min to ensure good electrical contact. The dielectric constant of the US-PZT was ∼1200.

Colloidal Probe Preparation. Colloidal probes were fabricated by attaching a 10 μm diameter borosilicate sphere with a mean surface roughness of 5.5 nm (Duke Scientific Cat: 9010) onto a Bruker NP "D" cantilever using Norland Products NOA 81 UV curing epoxy. The cantilever stiffness was determined from the thermal noise spectrum in air.[37] Prior to measurements, each colloidal probe was cleaned with a 1 min oxygen plasma ash followed by a 10 min immersion in Milli-Q water. This was followed by a 7 min exposure to UV/ozone before rinsing with ethanol and Milli-Q grade water.

Solution Preparation. All dilute electrolyte solutions were prepared and stored in clean glass vials. Dilute monovalent salt solutions were prepared using lithium chloride (CAS#10515-30), potassium chloride (CAS#87626-18), potassium nitrate (CAS#11008-14), and sodium chloride (CAS#7647-12-5). NaCl solutions were acidified with dilute HCl. Solution concentration and pH were measured using an Oakton Acron CON 5 Conductivity meter and an Oakton Ion 510 Series pH meter, respectively.

Force-Separation Measurements. Colloidal probe force microscopy measurements were performed using an Asylum Research MFP-3D scanning probe microscope. To avoid hydrodynamic forces, all force curves were collected with a tip speed of 400 nm s^{-1} (or less) over separation distances ranging from 500 to 1000 nm.[34] Once the colloidal probe and the sample were mounted in the AFM, a 150 μL droplet of electrolyte solution was placed on the US-PZT sample and held in place during measurements by capillary forces acting between the cantilever holder and the US-PZT surface. For each condition tested, force curves were taken using force-volume mapping over a 100 μm^2 area. The presented data uses a random selection of the measured force-separation curves. For each experimental condition, 12 curves were randomly selected for analysis. Obviously deviating curves were eliminated. Prior to polarization, CPFM force-separation curves were taken on the freshly annealed (native) US-PZT surface. The sample was then removed from solution, dried, and poled to express a negative surface charge. After poling, the sample was reimmersed in ionic solution for subsequent CPFM measurements while isolated from ground. Next, the polarized US-PZT sample was removed from solution, dried, and poled to express a positive surface charge. In all cases, the bottom electrode was isolated from ground. A new US-PZT sample was used for each ionic solution.

Polarization of US-PZT. Polarization of the FETF was performed ex situ by placing a clean, platinum coated silicon wafer on top of the US-PZT thin film surface and applying a ±40 V bias with a Keithley 6487 Piccoammeter/Voltage source (see Supporting Information). The US-PZT thin film was polarized to have a negative surface charge using a +40 V bias and polarized to have a positive surface charge using a −40 V bias. The surface of the US-PZT samples was uniformly polarized over an area of 1 cm^2. To ensure polarization saturation, the films were switched 10 times before the final polarization direction was induced. After the final polarization state was achieved, the bias was removed, the circuit was broken, and the top electrode was removed. This leads to free charges to persist in the bottom metal electrodes, which compensate the charges expressed by the bottom surface of the FETF. The charge density of the top surface on the ferroelectric film, on the other hand, remains uncompensated after removal of the top electrode, leading to an effective charge density equal to the remnant polarization of the FETF (σ_F). This uncompensated charge drives the formation of an EDL when the FETF is placed in an aqueous environment for CPFM measurement. We note that, when the bottom contact was grounded prior to placing the FETF in solution, the effective surface charge density of the FETF was negated.

Electric Double Layer Model and Fitting. The Derjaguin approximation was used to relate the normal force measured for a sphere-plate geometry (σ_{SP}) to the total interaction energy per unit area between two parallel plates (W_T) (eq 2)[24]

$$F_{SP} = 2\pi R W_T \tag{2}$$

where R is the colloidal probe radius (5 μm). The Derjaguin approximation is valid for our colloidal probe interacting with a flat plate because the inverse Debye length (κ) multiplied by the colloidal probe radius (R) is larger than 10 for all ionic strengths.[24,38]

The total interaction energy per unit area between two parallel plates (W_T) is obtained by the summation of van der Waals (W_V) and electrostatic interaction (W_E) energies (eq 3)

$$W_T = W_V + W_E \tag{3}$$

The nonretarded van der Waals interaction energy per unit area between two parallel plates was calculated by eq 4

$$W_V = \left(\frac{A^{132}}{12\pi d^2}\right) \tag{4}$$

where d is the separation distance and A^{132} is the Hamaker constant for two different solid surfaces (1, 2) interacting through a uniform medium (3). We used Lifshitz Theory[39,40] and commonly reported values for the refractive index of PZT[41,42] to determine a Hamaker constant of 0.66×10^{-20} J (see Supporting Information). This value agrees with previously reported values for oxide surfaces interacting through water.[43,44]

To determine the surface potential of the polarized US-PZT surface, we considered either a constant charge[45] or a constant potential[46] EDL model, derived from the linearized Poisson−Boltzmann equation (eq 5). We found that the constant charge EDL model consistently overpredicted the interaction force as a function of separation distance for known values of the inverse Debye length. The constant potential EDL model (eq 6), however, provided good fits to the measured force-separation data, indicating that a significant amount of charge regulation occurs at the US-PZT surface. Fitting the measured force-separation approach curves to a charge-regulation EDL model also indicates significant charge regulation (see Supporting Information).

$$\nabla^2\Psi = \kappa^2\Psi \tag{5}$$

$$W_E = \frac{\varepsilon_o\varepsilon_r\kappa}{8\pi}\{(\Psi_1^2 + \Psi_2^2)[1 - \coth(x)] + 2\Psi_1\Psi_2\operatorname{cosech}(x)\} \tag{6}$$

where Ψ_1 is the nondimensionalized potential ($\psi e/k_BT$) of the borosilicate probe, Ψ_2 is the nondimensionalized potential of the US-PZT surface, x is $2\kappa d$, $\varepsilon_o\varepsilon_r$ is the dielectric constant, $\kappa = [(2e_0^2 n)/(\varepsilon_o\varepsilon_r k_B T)]^{1/2}$ is the inverse Debye length, k_B is Boltzmann's constant, T is absolute temperature, and n is atomic concentration.

The total interaction force equation was determined by substituting eqs 3, 4, and 6 into eq 2. The total interaction force equation was fitted to the measured force-separation approach curves for native and polarized US-PZT thin films using a least-squares method and Tablecurve (Systat) software. During fitting, the Debye length (κ^{-1}) and the US-PZT surface potential (Ψ_2) were treated as fitting parameters while the surface potential of the borosilicate probe (Ψ_1)

was set to −39 mV. This surface potential was determined experimentally from colloidal force probe measurements on a silica surface and found not to change within the range of the ionic strengths used in the measurements (see Supporting Information). During sensitivity analysis, we found that changing the Hamaker constant by up to 1 order of magnitude did not significantly impact the fitting values (surface potential and Debye length). The measured force-separation data on approach were also compared with predictions from a nonlinear Poisson-Boltzmann model with a constant potential boundary condition.[47,48] However, we did not find a significant difference in the prediction of the US-PZT surface potentials. The surface charge at the OHP was calculated from the fitted surface potential values using the Grahame equation.[15,16]

Polarization Patterning. Charge patterning was performed using a clean TEM grid (Ted Pella 3HGC500). Uniform contact between the US-PZT surface and the TEM grid was made using a PDMS plug. A +40 V bias voltage was applied between the TEM grid and the bottom platinum electrode using a Keithley 6487 Piccoammeter/Voltage source. After the final polarization state was achieved, the potential difference between the top and bottom electrodes was brought to 0 V. The circuit was then broken, and the TEM grid was removed.

Colloidal Suspension Preparation. Colloidal suspensions were purchased from Invitrogen/Life Technologies. Aliphatic amine latex particles (100 nm diameter, 2% w/v, Product Number: A37358), express a positive surface charge in Milli-Q grade water. Carboxyl latex particles (400 nm diameter, 2% w/v, Product Number: C37268) express a negative surface charge in Milli-Q grade water. All colloidal suspensions were stored at 4 °C and protected from light. Prior to deposition, the colloidal suspension was warmed to room temperature and sonicated for 10 min at level 4.

Exposure to Colloidal Suspension. The polarization patterned US-PZT was exposed to a colloidal suspension using a double drop technique. First, a 150 μL drop of Milli-Q water or ionic solution was deposited onto the surface. Then, a 150 μL drop of colloidal suspension was pipetted onto the liquid droplet. Gentle mixing was performed using the micropipet to ensure solution homogeneity. By prewetting the US-PZT surface, we reduce nonspecific binding of colloidal particles onto the polarized US-PZT surface. After the desired exposure time is reached, the US-PZT surface was gently rinsed three times with Milli-Q grade water and dried with a stream of N_2.

Scanning Electron Microscopy Imaging. Clean dry samples of US-PZT were sputter coated (Denton Desk IV) with 20 nm of gold prior to scanning electron microscopy (SEM) imaging (FEI XL30 SEM-FEG) at 10 kV. The deposition process was observed with a Leica DM LFS microscope through an air immersion lens. The microscope phase contrast was adjusted to optimize imaging of the US-PZT surface.

RESULTS AND DISCUSSION

US-PZT Thin Film Surface. The interaction distance and strength of interfacial forces in aqueous liquids depend not only on surface charge characteristics, the ionic strength, and the material composition but also on surface roughness. Increases in surface roughness result in a decrease in the interaction force and an increase in the effective separation distance.[49,50] Preparation of ultrasmooth ferroelectric surfaces is thus necessary for the accurate measurement of electric double layer forces. Figure 3 presents the surface topography of US-PZT before and after submersion in Milli-Q grade water for 100 days. The mean surface roughness before and after water exposure is unchanged and has a value of 2.4 nm over a 25 μm^2 area. This demonstrates that, even after extended exposure, the US-PZT films are structurally stable in Milli-Q grade water. Reverse imaging of the borosilicate colloidal probe with SPM revealed a mean surface roughness of about 5 nm over a 25 μm^2 area.

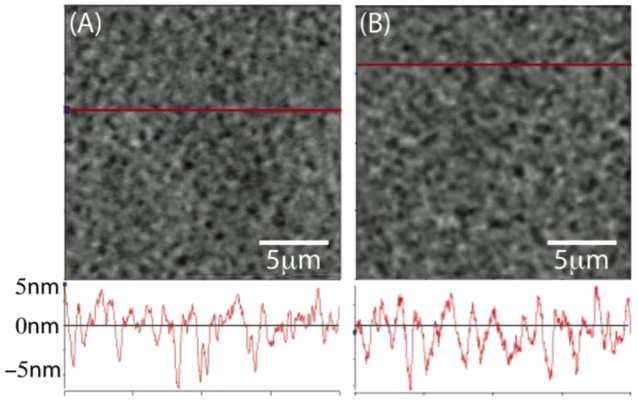

Figure 3. AFM contact mode images of our US-PZT surface (A) before and (B) after 100 days of exposure to Milli-Q grade water. The mean surface roughness and topography are unchanged. The lines indicate the location of the height profiles shown below the images.

Measurement of Electric Double Layer Forces of Native Ferroelectric Thin Films. Prior to polarization, CPFM measurements between a freshly annealed (native) US-PZT surface and a borosilicate colloidal probe were performed in Milli-Q grade water and in a variety of dilute electrolyte solutions. As shown in Figure 4, the type of 1:1

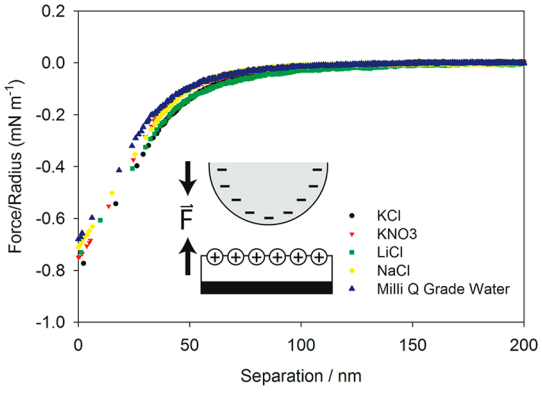

Figure 4. Force-separation approach curves for native US-PZT in Milli-Q water and in different types of 0.1 mM electrolyte solution. Force separation curves are normalized for colloidal probe radius.

electrolyte solution, at constant ionic strength, did not affect the attractive interaction force or distance between the borosilicate probe and the native US-PZT surface. This suggests that ion complexation does not affect the US-PZT surface potential and that the native, nonpoled US-PZT surface maintains a positive surface charge in aqueous environments. The positive surface charge agrees with previous acid/base titration experiments of lead oxide thin films and other ferroelectric perovskites.[51−53] This supports the conclusion that the native surface charge of the US-PZT arises from protonation of reactive surface sites. Using a constant potential boundary EDL model, we were able to determine the surface potential of the native US-PZT surface in aqueous solutions with different ionic strengths (Table 1).

Measurement of Electric Double Layer Forces of Polarized Ferroelectric Thin Films. Figure 5 shows force-separation approach curves for polarized US-PZT with a negative (Figure 5A) and positive surface charge (Figure 5B) for a range of NaCl concentrations. The long-range interaction between the negatively charged colloidal probe and the

Table 1. Average Fitted Values for a Constant Potential Boundary Condition EDL Model to CPFM Force-Separation Approach Curves for Polarized US-PZT in a Range of NaCl Electrolyte Solutions

concentration (mM)	measured Kappa^{-1} (nm)	Kappa^{-1} (nm)	OHP potential (mV)	OHP charge (μC/cm^{-2})	IHP potential (mV)	IHP charge (μC/cm^{-2})
Polarized US-PZT to Express a Negative Surface Charge						
0.01 ± 0.001	137.7 ± 0.5	129.8 ± 4.3	−63.8 ± 2.0	−0.035 ± 0.0006	−362 ± 2.0	−16.4 ± 0.001
0.1 ± 0.001	43.4 ± 0.02	34.8 ± 9.2	−37.0 ± 3.2	−0.081 ± 0.03	−334 ± 3.2	−16.5 ± 0.03
1.0 ± 0.1	14.6 ± 0.01	15.3 ± 8.5	−13.2 ± 3.6	−0.073 ± 0.03	−311 ± 3.6	−16.4 ± 0.03
Polarized US-PZT to Express a Positive Surface Charge						
0.01 ± 0.001	137.7 ± 0.5	83.1 ± 19.4	42.5 ± 0.6	0.005 ± 0.01	331 ± 0.6	15.9 ± 0.01
0.1 ± 0.001	43.4 ± 0.02	35.9 ± 5.9	32.0 ± 0.02	0.065 ± 0.01	320 ± 0.02	15.9 ± 0.01
1.0 ± 0.1	14.6 ± 0.01	13.2 ± 1.6	4.0 ± 0.8	0.02 ± 0.002	293 ± 0.8	15.9 ± 0.002
Native US-PZT						
0.01 ± 0.001	137.7 ± 0.5	194.9 ± 18.9	39.6 ± 2.9	0.014 ± 0.002		
0.1 ± 0.001	43.4 ± 0.02	29.8 ± 13.3	31.8 ± 1.4	0.092 ± 0.06		
1.0 ± 0.1	14.6 ± 0.01	10.4 ± 0.7	22.9 ± 3.6	0.156 ± 0.03		

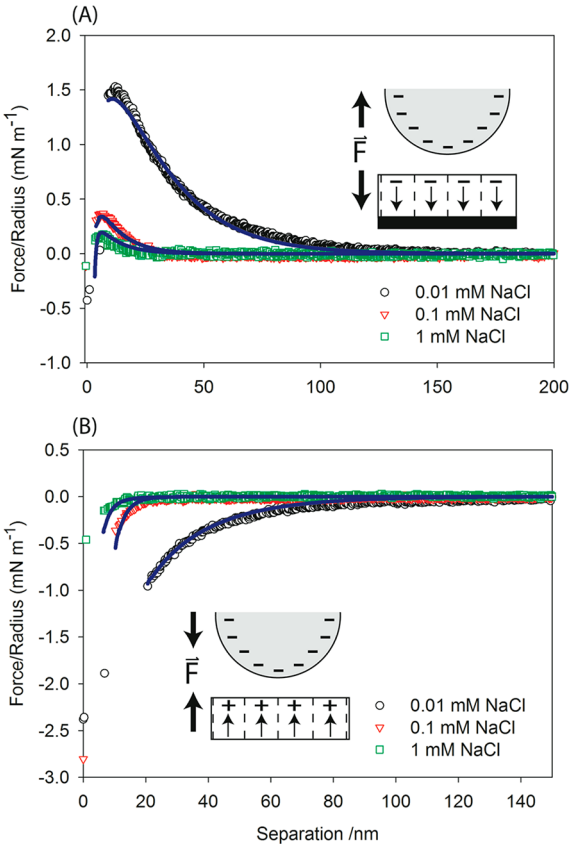

Figure 5. Force-separation approach curves for (A) a polarized US-PZT with a negative surface charge and (B) a polarized US-PZT with a positive surface charge, measured for a range of ionic strengths. The solid lines represent the best fit to the data calculated using a constant potential EDL model. Fitting values are shown in Table 1. A semilogarithmic plot for force-separation approach curve A is included in the Supporting Information.

polarized FETF with a negative surface charge was increasingly repulsive upon approach, until final snap-in occurred at close range. This long-range repulsive interaction is characteristic for overlapping EDLs between two like-charged surfaces. Although the native US-PZT surface has a positive charge, these results suggest that the polarization induced surface charges dominate the interaction energy.[54] Upon polarization reversal, the US-PZT has a positive surface charge and as a result its long-range interaction with the colloidal probe becomes increasingly attractive. Upon approach, this attractive interaction is characteristic for overlapping EDLs between oppositely charged surfaces. For both polarization states, the extent of the EDL interaction decreased with increasing ionic strength, as expected with the decreasing Debye length.[55−57] At ionic strengths above 10 mM, we were unable to resolve any further changes in the EDL interactions, because at these electrolyte concentrations, the Debye length (<2 nm) is smaller than the root-mean-square (RMS) surface roughness of the US-PZT (~2.4 nm) and the colloidal probe (~5 nm).[24] Short-range hydration forces were also not observed.[58,59]

In control experiments, we switched the polarization state of a US-PZT substrate repeatedly from a surface positive to a surface negative charge state and observed that the EDL interactions also switched accordingly. These experiments unequivocally demonstrate that the interaction behavior in aqueous environments is governed by the polarization state of the US-PZT films and not the charge state of the reactive surface sites.

The polarity observed on the US-PZT surface was opposite that one would have expected if mere charge injection had occurred. We thus conclude that the US-PZT surface charge is due to ferroelectric polarization.

We acquired XPS spectra before and after polarization to detect any polarization-induced surface chemical changes (e.g., oxidation or reduction) of the US-PZT thin film. Specifically, the binding energies of the oxygen 1s and the lead 4f peaks are sensitive to changes in the chemical bonding structure at the PZT surface.[17] Figure 6 presents high-resolution XPS spectra of the oxygen 1s and lead 4f regions region before and after polarization. Deconvolution of the oxygen 1s envelope reveals three binding moieties, which have been attributed to (I) adsorbed carbon containing species (e.g., −CO or −CO_2), (II) adsorbed oxygen, and (III) PbO.[60] Figure 6A shows that there is no significant change in the composition of oxygen binding moieties between the three samples. Furthermore, no significant difference in the doublet binding energy of the lead 2p envelope is apparent (Figure 6B). Taken together, these observations show that the chemical structure in the three samples does not change, which suggests that polarization does not induce appreciable changes in the chemical composition of the US-PZT surfaces.

To further demonstrate that the measured interaction forces primarily depend on the polarization state of the US-PZT, we

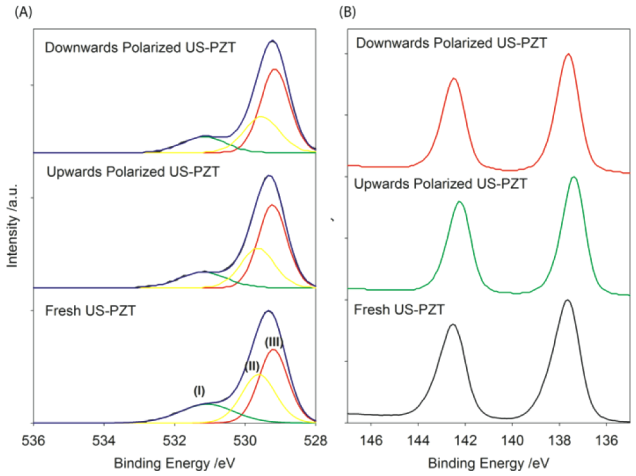

Figure 6. High resolution XPS spectra for (A) oxygen 1s and (B) lead 4f regions.

used CPFM experiments to test the effect of grounding the bottom platinum electrode of the US-PZT sample, which is expected to remove the free charge carriers on the bottom surface (see Supporting Information). While isolated from ground, the force-separation approach curves for native and polarized US-PZT with a negative surface charge reflect that the ferroelectric polarization state controls the EDL interaction force. Upon grounding, however, we observe that the effects of the polarization are removed and that the interaction again resembles that of native US-PZT. This effect is expected because of the small aspect ratio of the vertically polarized region within the US-PZT thin film. By grounding the bottom electrode, the free charges present in the metal, that were compensating the polarization charges at the bottom surface of the FETF, were drained and the remnant-field propagating from the polarized FETF became effectively negligible. Both the results of the XPS measurements and the disappearance of the EDL repulsion upon grounding demonstrate that the electric field propagating from the polarized FETF into the fluid results from the uncompensated charges present at the top surface of the ferroelectric (σ_F).

Electric Double Layer Modeling of Polarized US-PZT Surfaces. The measured force-separation approach curves between the polarized US-PZT surface and the colloidal probe were fitted to EDL theory using a constant potential boundary condition with a linearized Poisson–Boltzmann equation (Table 1). The theoretically predicted OHP potentials agree with values reported for metal oxide surfaces in aqueous environments.[55] Deviations of the theoretical fits from experimental results occur at small separation distances, which is common for EDL interaction force equations derived from a linearized Poisson–Boltzmann equation.[24] The fitted Debye lengths agree reasonably well those derived from the experimentally measured solution ionic strengths. Differences at low ionic strength may be attributed to water evaporation during measurement and experimental error. Previous work indicates that a Stern layer is present above polarized FETFs in both air and liquid.[6,23,61−63] The Stern layer can be composed of mobile surface charges, in the form or adsorbents (e.g., water or contaminants) or free charge carriers (e.g., oxygen vacancies or unit cell defect sites) on the surface.[64] By assuming the presence of a Stern layer, we calculated the IHP surface charge density of the US-PZT films. Using a linear capacitance across a condensed counterion layer,[24] we calculate IHP surface charge densities of −16.4 and 15.8 μC cm^{-2}. These values agree well with the independently measured remnant polarization values of our US-PZT of −16.3 and 15.3 μC cm^{-2} for both polarization states, respectively. The near symmetry in the magnitude of the surface charge density and the change in sign reflect the ability to switch the surface charge state of the FETF through polarization, thereby altering the probe−surface interactions.

Electric Double Layer Model Limitations. Although the force-separation approach curves were best fit by a constant potential boundary condition EDL model, charge-regulation processes may occur at the surface. Specifically, our use of a Stern layer to model the interaction force between a polarized FETF and a charged colloidal probe in solution may require the consideration of free charge carriers. Previous reports have supported that mobile charge carriers within the FETF may be capable of responding to externally applied electric fields.[6,7,62] Alternatively, the presence of a Stern layer has been shown capable of charge regulation.[44,59,65,66] To better model the effects of a charge regulation process, we have also fitted the measured force-separation approach curves using a linear-charge regulation model (see Supporting Information).[66] Our fitting results confirm that the US-PZT surface is charge regulating and that the IHP charge density matches the independently measured ferroelectric charge density. Overall, however, we find that the quality of fit between a charge regulation and a constant potential boundary condition EDL model are comparable, supporting the use of a constant potential boundary condition EDL model and the presence of a Stern layer.

Effects of Surface Roughness. Interfacial roughness on the US-PZT and colloidal probe can also decrease the measured interaction force in dilute electrolyte solutions and lead to under-prediction of the true surface charge density.[50,67,68] Even though our US-PZT thin films have a mean surface roughness of only 2.4 nm, the probe surface roughness was about 5 nm. The domain structure of a FETF results in nanoscale surface asperities (i.e., roughness) that increases the effective separation distance between surfaces and thus reduces the measured interfacial forces.[69,49] As such, domain size and crystallographic orientation are important considerations in integrating polarized FETFs for interfacial sensing applications in aqueous environments.

US-PZT Thin Films Stability at Low pH. We found that prolonged exposure of the native US-PZT surface to acidic solutions (pH < 4.2) induced a change from long-range attraction to long-range repulsion (Figure 7). Some interfacial softening was also observed (data not shown). Interfacial softening has been associated with the formation of a hydration layer on oxide surfaces.[70−73] The inversion of the interaction force observed here indicates a change in the chemical structure of the US-PZT surface.[51] This is consistent with reports of interfacial degradation of PZT after exposure to water vapor.[17,74] Furthermore, simple-oxide thin films have a lower point-of-zero charge, which may be responsible for the observed negative potential when placed in dilute electrolyte solutions.[57,75] Therefore, possible degradation of perovskite-structured ferroelectrics in high or low pH solutions needs to be considered further.

Guided Deposition of Charged Colloidal Particles Using Ferroelectrically-Induced Charge Patterns on US-PZT. To further demonstrate the ability for polarized US-PZT

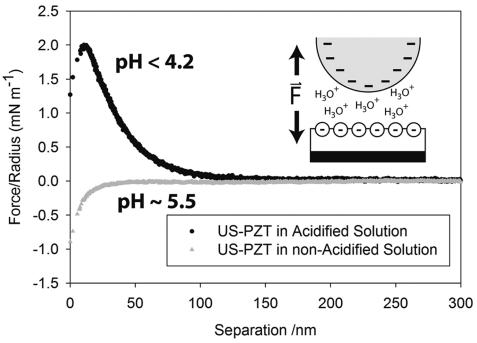

Figure 7. Native US-PZT in 10^{-4} M NaCl solution at pH 5.5 and 10^{-4} M NaCl solution at pH 4.2. The decrease in pH induces a long-range repulsion between the US-PZT and the negatively charged colloidal probe.

to control EDL interaction forces, we demonstrate the guided deposition of charged colloidal particles onto ferroelectrically induced surface charge patterns. Using a copper TEM grid, we locally polarized the US-PZT to have a negative surface charge. The nonpolarized regions of the US-PZT maintained a positive surface charge due to the native oxide surface. Figures 8A and B

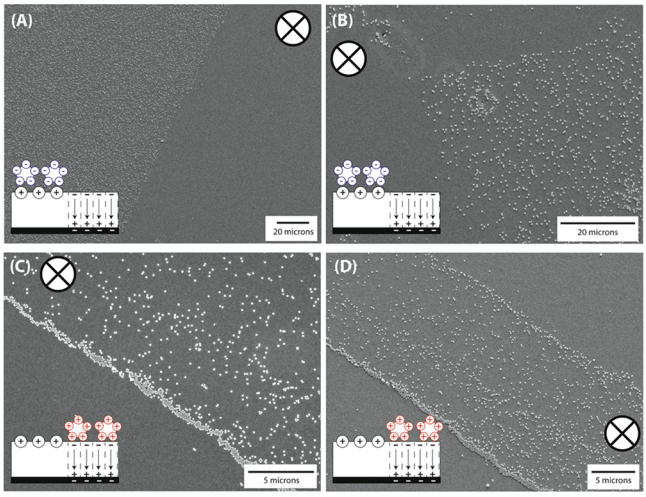

Figure 8. SEM images of charge-heterogeneous US-PZT after 3 h of exposure to (A and B) 400 nm, negatively charged, carboxyl terminated latex particles and (C and D) 100 nm, positively charged, amine terminated latex particles in Milli-Q grade water. In each image, we have included a deposition schematic and noted the local polarization direction.

show SEM images of the locally polarized US-PZT surface after incubation for 3 h with negatively charged colloidal latex particles (400 nm diameter) suspended in Milli-Q grade water. Figures 8C and D show SEM images of the locally polarized US-PZT surface after incubation for 3 h with positively charged colloidal latex particles (100 nm diameter) suspended in Milli-Q grade water. In both cases, we find that exposure of the charge-heterogeneous US-PZT surface to charged colloidal particles resulted in the charge selective deposition of the colloidal particles. Charge selective deposition patterns were absent when the US-PZT thin film was not polarized. However, some nonspecific deposition to like-charged regions of the US-PZT were observed, most likely arising during sample rinsing after particle deposition. Together, these observations demonstrate that the polarization state of the US-PZT is responsible for the charge selective deposition of colloidal particles and suggest that polarized FETFs can be used for charge-templated assembly applications.

CONCLUSIONS

We present the first study of an EDL induced by polarized ferroelectric US-PZT in dilute ionic solutions. We show that the surface charge density expressed by the ferroelectric polarization US-PZT thin films dominates over the native oxide surface. The ability to switch the polarization state of ferroelectric materials, i.e., switching their surface charge without altering other surface properties, makes this system attractive for isolating the effect of EDLs in the study of interfacial forces. The measured force-separation curves fit well to predictions by EDL theory using a constant potential boundary condition. With this model, we were able to determine the surface potential at the OHP for polarized US-PZT. Inclusion of a condensed Stern layer resulted in a match between the measured ferroelectric remnant polarization charge density and the calculated IHP charge density. Finally, we demonstrate the selective deposition of charged colloidal particles onto oppositely charged regions of our ferroelectric US-PZT. Our results are the first to quantify the interactions between polarized FETFs and colloidal materials and highlight the potential of FETFs for applications in guided deposition and interfacial sensing devices.

ASSOCIATED CONTENT

Supporting Information

Additional information on Hamaker constant calculation, control experiment results, and curve fitting with a charge-regulation EDL model. This material is available free of charge via the Internet at http://pubs.acs.org.

AUTHOR INFORMATION

Corresponding Author

*E-mail: zauscher@duke.edu. Telephone: (919) 660-5360.

Notes

The authors declare no competing financial interests.

ACKNOWLEDGMENTS

We thank Dr. Mark Wiesner and Dr. Hisham Massoud for valuable discussions. This research was supported by the National Science Foundation (NSF NIRT GRANT CBET-0609265, CMMI-0800769, and DMR-1121107 (MRSEC)). Furthermore, we thank Duke University for support of R.J.F. through both the GP-Nano and MRSEC fellowships.

REFERENCES

(1) Dawber, M.; Scott, J. F. *Rev. Mod. Phys.* **2005**, *77*, 1083−1130.
(2) Subbarao, E. C. *Ferroelectrics* **1973**, *5*, 267−280.
(3) Jones, R. E., Jr.; Maniar, P. D.; Moazzami, R.; Zurcher, P.; Witowski, J. Z.; Lii, Y. T.; Chu, P.; Gillespie, S. J. *Thin Solid Films* **1995**, *270*, 584−588.
(4) Paz De Araujo, C.; Scott, J. F. Taylor, G. W. *Ferroelectric thin films: synthesis and basic properties*; Gordon and Breach: Amsterdam, Holland, 1996; p 135.
(5) Sergei, V. K.; Anna, N. M.; Long Qing, C.; Brian, J. R. *Rep. Prog. Phys.* **2010**, *73*, 056502−056569.
(6) Kalinin, S. V.; Bonnell, D. A. *Phys. Rev. B.* **2001**, *63*, 125411−125424.
(7) Kalinin, S. V.; Bonnell, D. A. *Nano Lett.* **2004**, *4*, 555−560.

(8) Setter, N.; Damjanovic, D.; Eng, L.; Fox, G.; Gevorgian, S.; Hong, S.; Kingon, A.; Kohlstedt, H.; Park, N. Y.; Stephenson, G. B.; Stolitchnov, I.; Taganstev, A. K.; Taylor, D. V.; Yamada, T.; Streiffer, S. *J. Appl. Phys.* **2006**, *100*, 051606−051646.
(9) Heyman, P. M.; Heilmeier, G. H. *Proc. IEEE* **1966**, *54*, 842−848.
(10) Ferris, R.; Yellen, B.; Zauscher, S. *Small* **2012**, *8*, 28−35.
(11) Van Der Heyden, F. H. J.; Stein, D.; Dekker, C. *Phys. Rev. Lett.* **2005**, *95*, 116104.
(12) Tien, J.; Terfort, A.; Whitesides, G. M. *Langmuir* **1997**, *13*, 5349−5355.
(13) Biddiss, E.; Erickson, D.; Li, D. *Anal. Chem.* **2004**, *76*, 3208−3213.
(14) Boström, M.; Williams, D. R. M.; Ninham, B. W. *Phys. Rev. Lett.* **2001**, *87*, 168103−168107.
(15) Christenson, H. K. *J. Chem. Soc. Faraday Trans. 1* **1984**, *80*, 1933−1946.
(16) Grasso, D.; Subramaniam, K.; Butkus, M.; Strevett, K.; Bergendahl, J. *Rev. Env. Sci. Biotechnol.* **2002**, *1*, 17−38.
(17) Fujisaki, Y.; Torii, K.; Hiratani, M.; Kushida-Abdelghafar, K. *Appl. Surf. Sci.* **1997**, *108*, 365−369.
(18) Cooney, T. G.; Francis, L. F. *J. Micromech. Microeng.* **1996**, *6*, 291−298.
(19) Navarro, A.; Rocks, S. A.; Dorey, R. A. *J. Electroceram.* **2007**, *19*, 321−326.
(20) Nir, S. *Soil Sci. Soc. Am. J.* **1986**, *50*, 52−57.
(21) Nir, S.; Hirsch, D.; Navrot, J.; Banin, A. *Soil Sci. Soc. Am. J.* **1986**, *50*, 40−45.
(22) Miller, S. E.; Low, P. F. *Langmuir* **1990**, *6*, 572−578.
(23) Jones, P. M.; Dunn, S. *J. Phys. D: Appl. Phys.* **2009**, *42*, 065408−065413.
(24) Israelachvili, J. N. *Intermolecular and surface forces*; Academic Press: London; San Diego, 1991; p 215.
(25) Mosley, L. M.; Hunter, K. A.; Ducker, W. A. *Environ. Sci. Technol.* **2003**, *37*, 3303−3308.
(26) Kim, J.; Nason, J. A.; Lawler, D. F. *Environ. Sci. Technol.* **2008**, *42*, 2557−2562.
(27) Yuqing, M.; Jianguo, G.; Jianrong, C. *Biotechnol. Adv.* **2003**, *21*, 527−534.
(28) Cahill, B. P.; Heyderman, L. J.; Gobrecht, J.; Stemmer, A. *Phys. Rev. E* **2004**, *70*, 036305.
(29) Luckham, P. F. *Adv. Colloid Interface Sci.* **2004**, *111*, 29−47.
(30) Behrens, S. H.; Grier, D. G. *J. Chem. Phys.* **2001**, *115*, 6716−6721.
(31) Hiemstra, T.; De Wit, J. C. M.; Van Riemsdijk, W. H. *J. Colloid Interface Sci.* **1989**, *133*, 105−117.
(32) Yates, D. E.; Levine, S.; Healy, T. W. *J. Chem. Soc. Faraday Trans. 1* **1974**, *70*, 1807−1818.
(33) Horne, D. S.; Davidson, C. M. *Colloid Polym. Sci.* **1986**, *264*, 727−734.
(34) Zauscher, S.; Klingenberg, D. J. *J. Colloid Interface Sci.* **2000**, *229*, 497−510.
(35) Pashley, R. M.; Israelachvili, J. N. *J. Colloid Interface Sci.* **1984**, *97*, 446−455.
(36) Xia, D.; Liu, M.; Zeng, Y.; Li, C. *Mater. Sci. Eng.* **2001**, *87*, 160−163.
(37) Sader, J. E.; Chon, J. W. M.; Mulvaney, P. *Rev. Sci. Instrum.* **1999**, *70*, 3967−3969.
(38) Lin, S.; Wiesner, M. *Langmuir* **2010**, *26*, 16638−16641.
(39) Dzyaloshinskii, I. E.; Lifshitz, M.; Pitaevskii, L. P. *Phys.-Usp.* **1961**, *4*, 153−176.
(40) Visser, J. *Adv. Colloid Interface Sci.* **1972**, *3*, 331−363.
(41) Aulika, I.; Corkovic, S.; Bencan, A.; D'astorg, S.; Dejneka, A.; Zhang, Q.; Kosec, M.; Zauls, V. *J. Electrochem. Soc.* **2009**, *156*, G217−G225.
(42) Aulika, I.; V, Z.; Kundzins, K.; Kundzins, M.; Katholy, S. *J. Optoelectron. Adv. Mater.* **2003**, *5*, 755 −761.
(43) Larson, I.; Drummond, C. J.; Chan, D. Y. C.; Grieser, F. *J. Phys. Chem.-US* **1995**, *99*, 2114−2118.
(44) Behrens, S. H.; Borkovec, M. *J. Phys. Chem. B* **1999**, *103*, 2918−2928.
(45) John, G. *J. Colloid Interface Sci.* **1975**, *51*, 44−51.
(46) Hogg, R.; Healy, T. W.; Fuerstenau, D. W. *Trans. Faraday Soc.* **1966**, *62*, 1638−1651.
(47) Dunér, G.; Iruthayaraj, J.; Daasbjerg, K.; Pedersen, S. U.; Thormann, E.; Dėdinaitė, A. *J. Colloid Interface Sci.* **2012**, *385*, 225−234.
(48) Blomberg, E.; Claesson, P. M.; Froeberg, J. C.; Tilton, R. D. *Langmuir* **1994**, *10*, 2325−2334.
(49) Bhattacharjee, S.; Ko, C.-H.; Elimelech, M. *Langmuir* **1998**, *14*, 3365−3375.
(50) Considine, R. F.; Drummond, C. J. *Langmuir* **2001**, *17*, 7777−7783.
(51) Paik, U.; Lee, S.; Hackley, V. A. *J. Am. Ceram. Soc.* **2003**, *86*, 1662−1668.
(52) Hanawa, T.; Kon, M.; Doi, H.; Ukai, H.; Murakami, K.; Hamanaka, H.; Asaoka, K. *J. Mater. Sci.: Mater. Med.* **1998**, *9*, 89−92.
(53) Carre, A.; Roger, F.; Varinot, C. *J. Colloid Interface Sci.* **1992**, *154*, 174−183.
(54) Chan, D. Y. C. *J. Colloid Interface Sci.* **2002**, *245*, 307−310.
(55) Ducker, W. A.; Senden, T. J.; Pashley, R. M. *Nature* **1991**, *353*, 239−241.
(56) Hunter, R. J. *Foundations of colloid science*; Oxford University Press: Oxford; New York, 2001; Vol. *1*, p 435.
(57) Larson, I.; Drummond, C. J.; Chan, D. Y. C.; Grieser, F. *J. Am. Chem. Soc.* **1993**, *115*, 11885−11890.
(58) Grabbe, A.; Horn, R. G. *J. Colloid Interface Sci.* **1993**, *157*, 375−383.
(59) Pashley, R. M. *J. Colloid Interface Sci.* **1981**, *83*, 531−546.
(60) Fujisaki, Y.; Kushida-Abdelghafar, K.; Miki, H.; Shimamoto, Y. *Integr. Ferroelectr.* **1998**, *21*, 83−95.
(61) Kalinin, S. V.; Bonnell, D. A. *Appl. Phys. Lett.* **2001**, *78*, 1116−1118.
(62) Shin, J.; Nascimento, V. B.; Geneste, G. G.; Rundgren, J.; Plummer, E. W.; Dkhil, B.; Kalinin, S. V.; Baddorf, A. P. *Nano Lett.* **2009**, *9*, 3720−3725.
(63) Chen, X. Q.; Yamada, H.; Horiuchi, T.; Matsushige, K.; Watanabe, S.; Kawai, M.; Weiss, P. S. *J. Vac. Sci. Technol., B* **1999**, *17*, 1930−1934.
(64) Li, X.; Mamchik, A.; Chen, I. W. *Appl. Phys. Lett.* **2001**, *79*, 809−811.
(65) Biesheuvel, P. M. *J. Colloid Interface Sci.* **2004**, *275*, 514−522.
(66) Chan, D. Y. C.; Healy, T. W.; Supasiti, T.; Usui, S. *J. Colloid Interface Sci.* **2006**, *296*, 150−158.
(67) Kostoglou, M.; Karabelas, A. J. *J. Colloid Interface Sci.* **1995**, *171*, 187−199.
(68) Suresh, L.; Walz, J. Y. *J. Colloid Interface Sci.* **1996**, *183*, 199−213.
(69) Hoek, E. M. V.; Agarwal, G. K. *J. Colloid Interface Sci.* **2006**, *298*, 50−58.
(70) Minor, M.; Van Der Linde, A. J.; Van Leeuwen, H. P.; Lyklema, J. *Colloids Surf., A* **1998**, *142*, 165−173.
(71) Vigil, G.; Xu, Z.; Steinberg, S.; Israelachvili, J. *J. Colloid Interface Sci.* **1994**, *165*, 367−385.
(72) Kobayashi, M.; Juillerat, F.; Galletto, P.; Bowen, P.; Borkovec, M. *Langmuir* **2005**, *21*, 5761−5769.
(73) Campen, R. K.; Pymer, A. K.; Nihonyanagi, S.; Borguet, E. *J. Phys. Chem. C* **2010**, *114*, 18465−18473.
(74) Kim, K. S.; O'Leary, T. J.; Winograd, N. *Anal. Chem.* **1973**, *45*, 2214−2218.
(75) Van Oss, C. J. *Interfacial forces in aqueous media*; Taylor & Francis: Boca Raton, FL, 2006; Vol. *1*, p 25.